Structural basis of the transmembrane domain dimerization and rotation in the activation mechanism of the TRKA receptor by nerve growth factor

Received for publication, October 1, 2019, and in revised form, November 26, 2019 Published, Papers in Press, December 4, 2019, DOI 10.1074/jbc.RA119.011312

María L. Franco[‡1], Kirill D. Nadezhdin[§¶1], Sergey A. Goncharuk[§¶], Konstantin S. Mineev[§¶], Alexander S. Arseniev[§¶2], and Marçal Vilar[‡3]

From the [‡]Molecular Basis of Neurodegeneration Unit, Institute of Biomedicine of València, Consejo Superior de Investigaciones Científicas, 46010 València, Spain, the [§]Shemyakin-Ovchinnikov Institute of Bioorganic Chemistry, Russian Academy of Sciences, Moscow 117997, Russian Federation, and the [¶]Moscow Institute of Physics and Technology (State University), Institutskiy Pereulok 9, Dolgoprudny, Moscow Region 141700, Russian Federation

Edited by Karen G. Fleming

Tropomyosin-receptor kinases (TRKs) are essential for the development of the nervous system. The molecular mechanism of TRKA activation by its ligand nerve growth factor (NGF) is still unsolved. Recent results indicate that at endogenous levels most of TRKA is in a monomer–dimer equilibrium and that the binding of NGF induces an increase of the dimeric and oligomeric forms of this receptor. An unsolved issue is the role of the TRKA transmembrane domain (TMD) in the dimerization of TRKA and the structural details of the TMD in the active dimer receptor. Here, we found that the TRKA–TMD can form dimers, identified the structural determinants of the dimer interface in the active receptor, and validated this interface through site-directed mutagenesis together with functional and cell differentiation studies. Using *in vivo* cross-linking, we found that the extracellular juxtamembrane region is reordered after ligand binding. Replacement of some residues in the juxtamembrane region with cysteine resulted in ligand-independent active dimers and revealed the preferred dimer interface. Moreover, insertion of leucine residues into the TMD helix induced a ligand-independent TRKA activation, suggesting that a rotation of the TMD dimers underlies NGF-induced TRKA activation. Altogether, our findings indicate that the transmembrane and juxtamembrane regions of TRKA play key roles in its dimerization and activation by NGF.

Nerve growth factor (NGF)[4] is a member of the mammalian neurotrophin protein family implicated in the maintenance and survival of the peripheral and central nervous systems (1–3). NGF is a dimer that interacts with two distinct receptors: TRKA, a cognate member of the Trk receptor tyrosine kinase family, and the p75 neurotrophin receptor, which belongs to the tumor necrosis factor receptor superfamily of death receptors (4–6). TRKA signaling is essential for sensory and sympathetic neuron survival during development (7). Genetic mutations in the gene that encodes TRKA, *NTRK1*, cause congenital insensitivity to pain with anhidrosis (8), and somatic mutations and chromosomal rearrangements generate aberrant protein fusions with constitutive kinase activation causing several types of cancer (9, 10).

Despite all these important roles, the molecular mechanisms of TRKA activation have been poorly studied compared with those of other receptor-tyrosine kinase (RTK) family members (11, 12). The first three extracellular domains of TRKA consist of a leucine-rich region (Trk-d1) that is flanked by two cysteine-rich domains (Trk-d2 and Trk-d3). The fourth and fifth domains (Trk-d4 and Trk-d5) are Ig-like domains, and they are followed by a 30-residue-long linker that connects the extracellular portion of the receptor to the single transmembrane domain and a juxtamembrane intracellular region that is connected to the kinase domain. TRKA is activated by NGF a member of the neurotrophin family (3). The NGF-binding domain is located in the Trk-d5(Ig2) domain (13), although other domains also participate in the activation by neurotrophins through an unknown mechanism (14, 15).

Two models for TRKA activation are postulated; a ligand-induced dimerization of TRKA monomers and a ligand-induced conformational activation of preformed inactive dimers. The first model, which is based on the crystal structure of NGF with the ligand-binding domain of TRKA (13, 16), assumed that

This work was supported by the Ministerio de Economía, Industria y Competitividad Projects BFU2013-42746-P and SAF2017-84096-R and by Generalitat Valenciana Prometeo Grant 2018/055 (to M. V.). The studies of TRKA-TM homodimerization were supported by Russian Science Foundation Grant 19-74-30014 (to A. S. A). The authors declare that they have no conflicts of interest with the contents of this article.

This article contains Table S1 and Figs. S1–S7.

The atomic coordinates and structure factors (code 2n90) have been deposited in the Protein Data Bank (http://wwpdb.org/).

The NMR chemical shift data of this paper are available from the Biological Magnetic Resonance Data Bank under BMRB accession number 25872.

[1] These authors contributed equally to this work.

[2] To whom correspondence may be addressed: Shemyakin-Ovchinnikov Institute of Bioorganic Chemistry of the Russian Academy of Sciences, Moscow 117997, Russian Federation. E-mail: aars@nmr.ru.

[3] To whom correspondence may be addressed: Neurodegeneration Unit, Institute of Biomedicine CSIC, C/ Jaume Roig 11, 46010 València, Spain. E-mail: mvilar@ibv.csic.es.

[4] The abbreviations used are: NGF, nerve growth factor; TRK, tropomyosin-receptor kinase; TM, transmembrane; TMD, TM domain; JTM, juxtamembrane; eJTM, extracellular JTM; RTK, receptor-tyrosine kinase; ICD, intracellular domain; DPC, dodecylphosphocholine; DPR, detergent-to-protein molar ratio; HSQC, heteronuclear single quantum coherence; eJTM, extracellular juxtamembrane region; PEI, polyethylenimine; ANOVA, analysis of variance.

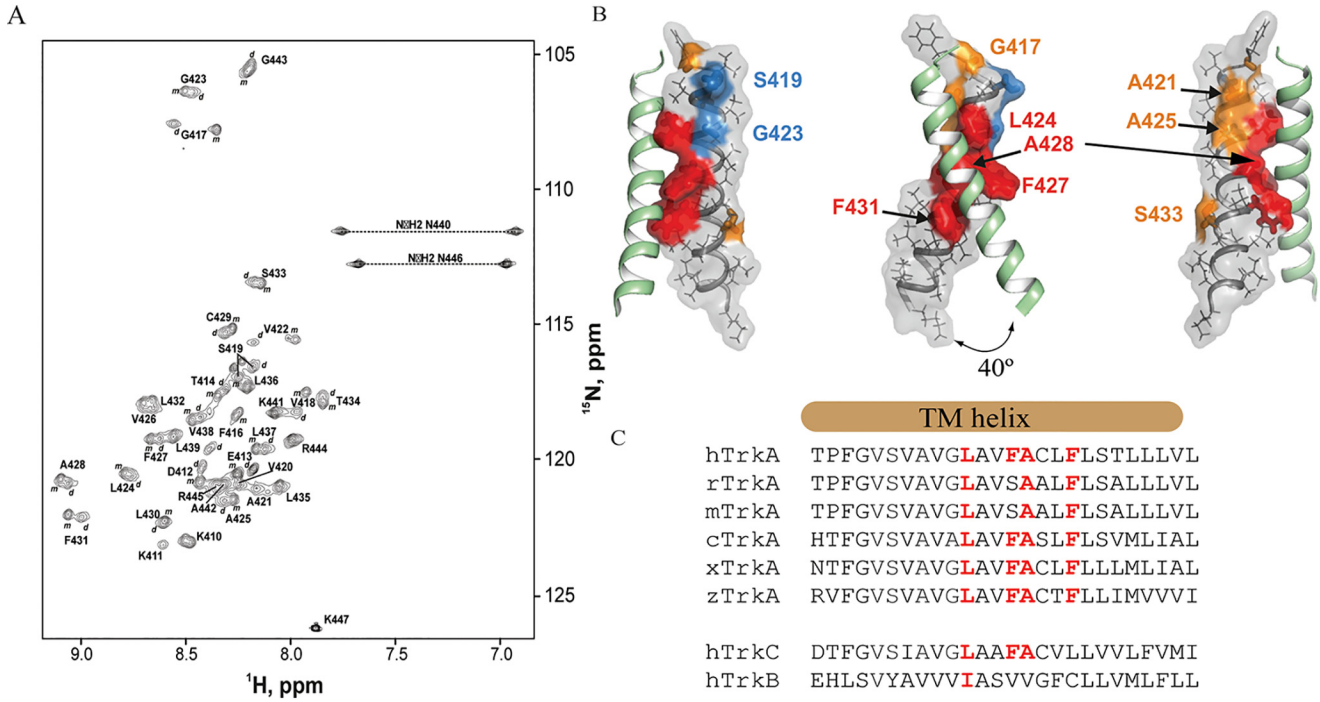

Figure 1. NMR structure of TRKA transmembrane domain dimers in DPC micelles. *A*, the ^{1}H/^{15}N HSQC spectrum of the human TRKA–TMD-wt. The human TRKA–TMD was solubilized in an aqueous suspension of DPC micelles at a DPR of 50:1 and at 45 °C and pH 5.9. ^{1}H–^{15}N backbone and side-chain resonance assignments are shown. *B*, schematic representation of the NMR spatial structure of the human TRKA–TMD dimer in detergent micelles, from different angles. The surface of one TMD helix is represented with the NMR dimer interface in *red*. The TMD of the other monomer within the dimer is represented as *ribbons*, and side chains are indicated as *sticks*. The location of the NMR dimer interface L*XX*FA*XX*F on the NMR structure is colored *red*, and other mutated residues are colored *orange*. The putative dimerization motif S*XXX*G is shown in *blue*. The Protein Data Bank accession code is 2n90. *C*, alignment of the amino acid sequences of the transmembrane helical domain of TRKA from different species (*h*, *Homo sapiens*; *r*, *Rattus norvegicus*; *m*, *Mus musculus*; *c*, *Gallus gallus*; *z*, *Danio rerio*; *x*, *Xenopus laevis*). The residues participating in the NMR dimer interface are highlighted in *red*.

the dimerization of TRKA is solely ligand-mediated and that receptor–receptor interactions are not present in the absence of its ligand. In the second model, TRKA exists as a preformed inactive dimer, suggesting receptor–receptor contacts in the absence of NGF (17, 18). The most recent data using single-particle tracking (19) and FRET studies (20) suggest that TRKA is, at endogenous levels, predominantly monomer (80%), and NGF binding induces an increase and a stabilization of the TRKA dimers and the formation of oligomers, together with a conformational change leading to kinase activation. This mechanism of activation has been called the "transition model" (20) and postulates a dynamic transition from a monomer to an inactive dimer to a ligand-bound active dimer, suggesting that Trk receptors are activated through a combination of the two mentioned models.

Whatever the model, it is clear that dimerization of TRKA is required for its activation. Deletion constructs suggested that dimerization of TRKA is mediated by the transmembrane (TM) and by the intracellular domains (ICDs) (20). In the case of the ICDs, this is supported by the crystal structure of the kinase domain of TRKA that showed the presence of dimers in the crystallographic unit (21, 22). However, the structural determinants of the TMD dimerization are not known, and in this regard, it is important to understand the conformation of the TRKA–TMD dimer and identify the active dimer interface that may represent the functional state of the full-length receptor. In addition biochemical data supporting a conformational activation of TRKA are lacking. In the present work, we investigated the structural basis of TRKA–TMD dimerization in the activation of TRKA by NGF, using complementary structural and biochemical approaches.

Results

Structure of TRKA transmembrane domain dimers

It has been shown that the isolated TMDs of all human RTKs form dimers in bacterial membranes (23). In addition functional studies indicate that TMDs play an important role as a modulator of RTK homodimerization and kinase activation (reviewed in Refs. 23–25). Switching between two dimerization modes of the transmembrane helix has recently been described as part of the activation mechanism of the epidermal growth factor, vascular endothelial growth factor, and fibroblast growth factor receptors (26–29). However, to date the role of TRKA–TMD dimerization in TRKA receptor activation has not been studied in detail.

To obtain a structural insight into TRKA–TMD dimerization, we solved the structure of human TRKA–TMD dimers in detergent micelles using NMR (Fig. 1). For this study, the human TRKA–TMD was produced in a cell-free system (see "Experimental procedures") as previously described (30). When the peptide is solubilized in dodecylphosphocholine (DPC) micelles at a detergent-to-protein molar ratio (DPR) of 50:1, the TRKA–TMD is in equilibrium between monomeric, dimeric, and other oligomeric states. The ratio of these states varies as the DPR value is altered (Fig. S1*A*). We then titrated TRKA–

TMD in DPC micelles to measure the standard free energy of dimerization (ΔG_0) using standard methods (31) (see details under "Experimental procedures" and Fig. S1*B*). The ΔG_0 value obtained (-1.9 ± 0.2 kcal/mol) suggested that the TRKA–TMD dimer is quite stable compared with the TMD dimers of other RTKs. Thus, although its dimerization energy is weaker than that of the vascular endothelial growth factor receptor 2 dimer ($\Delta G_0 = -2.5$ kcal/mol in DPC) (32), it is stronger than those of fibroblast growth factor receptor 3 ($\Delta G_0 = -1.4$ kcal/mol in DPC/SDS 9:1 mixture) and ErbB4 ($\Delta G_0 = -1.4$ kcal/mol in DMPC/DHPC 1:4 bicelles) (33). The ^{15}N HSQC spectrum of ^{15}N-labeled TRKA–TMD (Fig. 1*A*) contained the expected number of cross-peaks, and the good quality of the spectra allowed solving of the structure of the dimer in DPC micelles (Figs. 1*B*, Figs. S2–S4, and Table S1). The α-helical region of the TRKA-TM dimer starts at Gly^{417}, ends at Asn^{440}, and is ~38 Å in length (Fig. S2). The crossing angle of the TRKA-TM helices is 40°, and the minimal distance between two monomers is 8.8 Å (Fig. 1*B* and Table S1). The hydrophobicity plot and contact surface area of the dimer is shown in Fig. S4. The dimerization interface lies along the sequence motif ^{424}L*XX*FA*XX*F^{431} (Fig. 1*B* and Fig. S4) that is conserved in the TRKA–TMD of several species and also in TrkC but not in TrkB (Fig. 1*C*). Although the TRKA–TMD sequence contains a putative dimerization motif of the form S*XXX*G (shown in *blue* in Fig. 1*B*), this motif resides in an opposite helix interface.

These analyses of TRKA–TMD dimerization suggested the existence of the dimerization motif ^{424}L*XX*FA*XX*F^{431} (Fig. 1*B*). The biological relevance of this motif can be questioned, because the presence of large extracellular and intracellular globular domains or the lipid environment of the plasma membrane may favor or hinder a specific interaction interface (34). We therefore used different functional assays to verify the found dimer interface in the context of the full-length receptor.

Functional identification of the dimer interface upon NGF stimulation

The state of full-length TRKA was followed by assay of three different aspects of its activity: dimerization of the receptor, phosphorylation of intracellular tyrosine residues, and neurite differentiation of PC12nnr5 cells. To investigate the dimerization of TRKA, we individually mutated most of the N-terminal residues of the rat TRKA–TMD to cysteine (Fig. 2*A*), expressed these constructs in HeLa cells, and then measured the amount of cross-linked species. To facilitate cross-linking via these cysteine residues in the transmembrane domains, we used oxidation with molecular iodine (I_2) as previously described (35). Such oxidation allows the formation of a disulfide bond between two close cysteine residues inside the lipid bilayer. Plasma membrane fractions from cells expressing different single-cysteine mutants were incubated in the absence or presence of NGF, together with molecular I_2 and were then analyzed by nonreducing SDS-PAGE and Western immunoblotting. Upon transfection in HeLa cells, the mutants G417C and V418C formed covalent dimers in the absence of NGF (Fig. 2, *B* and *C*). NGF stimulation increased the amount of G417C and V418C dimers, and low quantities of dimers in the V420C, A421C, and V422C mutants were observed (Fig. 2, *B* and *C*). Overexpression of TRKA induces a ligand-independent activation. To see whether the constitutive dimerization of some of these mutants induces the activation of TRKA, we transfected the cysteine mutants in PC12nnr5 cells and studied the differentiation in NGF-independent manner. As we can see in Fig. 2*D*, only the mutant V418C is able to induce the differentiation in the absence of NGF, suggesting that V418C is part of the active dimer interface.

To further study the significance of the found interfaces, we mutated the small residues Ala, Gly, and Ser within this region to the bulky Ile residue, and we then assayed TRKA activation upon NGF stimulation (Fig. 2, *E* and *F*). The rationale behind this approach was that the mutation of a small residue to a bulky one on the relevant interface would prevent the formation of the active dimeric state by inducing steric clashes and would therefore reduce TRKA activation. To perform this assay, we transfected HeLa cells that do not express endogenous TRKA with these mutants, stimulated these cells with nonsaturating concentrations (10 ng/ml) of NGF, and then assayed TRKA activation by analysis of TRKA autophosphorylation using Western blotting. Upon transfection, two TRKA electrophoretic bands are present in the TRKA immunoblots of HeLa cells: a lower band (~110 kDa) of intracellular immature TRKA that has not completed Golgi-mediated processing of high-mannose *N*-glycans (36) and an upper band (~140 kDa) with mature sugars that is expressed in the plasma membrane. Exposure to NGF substantially increased the phosphorylation of the upper TRKA band as assessed by blotting with a phospho-specific antibody against the phosphotyrosine residues of the activation loop, P-Tyr^{674} and P-Tyr^{675}. This autophosphorylation was quantified to follow TRKA activation. Constitutive ($t = 0$, no NGF added) and ligand-dependent phosphorylation of plasma membrane-localized TRKA after 5 and 15 min were measured. Because overexpression of TRKA induces ligand-independent autophosphorylation, we first transfected the HeLa cells with increasing concentrations of TRKA to determine a TRKA level that could still be detected but that displayed no autophosphorylation in the upper band in the absence of NGF (Fig. S5). It is noteworthy that all mutants are expressed at the plasma membrane as evidenced by immunofluorescence localization in the absence of Triton X-100 using an antibody against an epitope in the TRKA N terminus (Fig. S6) and by flow cytometry (Fig. 2*F*). Of the seven single-point mutants tested, only the A428I substitution demonstrated a pronounced inhibitory effect on receptor autophosphorylation (Fig. 2*E*). Ala^{428} is the only small-chain residue that is found deep and in the closest position in the dimerization interface of the TRKA TMD structure determined using NMR, which supports the relevance of the obtained NMR structure. The inhibitory effect of A428 substitution on receptor activity was further enhanced when all three Ala residues that are at least somehow involved in the TMD dimerization in the NMR-based structure: Ala^{421}, Ala^{425}, and Ala^{428}, were simultaneously substituted (TRKA-3A/3I).

Lastly, we studied the effect of the same mutations on the NGF-induced differentiation of transfected PC12nnr5 cells

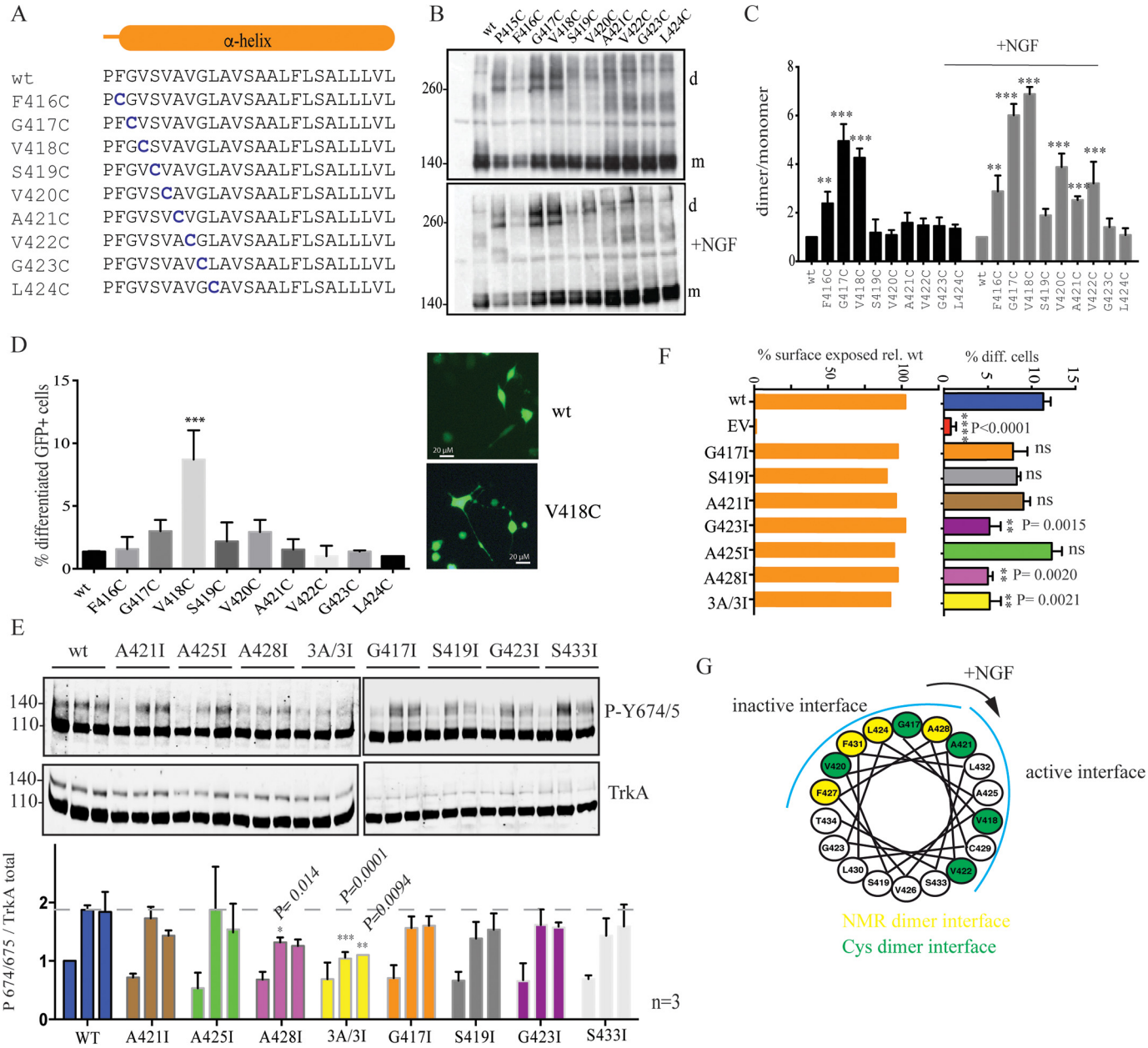

Figure 2. Functional identification of the active dimer interface in the TRKA–TMD. *A*, amino acid sequence of the transmembrane domain of rat TRKA showing the location of the single cysteine residue substitutions. *B*, Western blotting of HeLa cells transfected with the indicated TRKA–TMD constructs and analyzed using nonreducing SDS-PAGE, showing the formation of covalent cysteine dimers (*d*) arising from monomers (*m*) cross-linked using molecular iodine (I_2) in the presence or absence of NGF. *C*, quantification of the data in *B* derived from at least three independent experiments. *Bars* represent standard error of the mean. Statistics were performed using two-way ANOVA and Dunnett's multiple comparison test using GraphPad software. ****, $p < 0.0001$; ***, $p = 0.0004$. *D*, PC12nnr5 cells were transfected with the indicated constructs and 48 h later analyzed for the presence of neurites. The percentage of cells with at least one neurite longer than the cell body was quantified. At right fluorescence microscopy showing the formation of neurites in the PC12nnr5 cells co-transfected with TRKA and GFP. *E*, *top panel*, HeLa cells transfected with the indicated TRKA constructs were stimulated with NGF (10 ng/ml) for 0, 5, or 15 min. The immunoblots show the activation (autophosphorylation) of TRKA as detected using an antibody specific for TRKA P-Tyr$^{674/675}$. The levels of total TRKA are shown *below* each blot. Molecular weight markers are shown at *left*. *Bottom panel*, quantification of the data from the *top panel* derived from at least three independent experiments. *Bars* represent standard error of the mean. Statistics were performed using two-way ANOVA and Dunnett's multiple comparison test using GraphPad software. *p* values of conditions significantly different from WT are shown on *top* of the *error bars*. *F*, cytometric analysis of the expression of the TRKA mutants at the plasma membrane (*orange bars*) and quantification of the percentage of PC12nnr5 differentiated cells (*multicolored bars*) transfected with the indicated TRKA constructs together with GFP. *EV*, empty vector. The percentage of the total GFP-positive transfected cells with a neurite twice as long as the length of the cell body was quantified. *G*, helical wheel model of the TRKA–TMD showing the two dimer interfaces identified by NMR and by functional studies. An *arrow* shows the putative rotation from the two interfaces. *Bars* represent the standard error of at least three independent experiments. Statistical analysis was performed using ordinary one-way ANOVA, using Bonferroni's multicomparison test compared with wt. The *p* values of significant differences are shown. *ns*, not significant.

(Fig. 2*H*). Again, the A428I mutant displayed substantial inhibition of this TRKA activity. Unexpectedly the mutation G423I did have an impact on cell differentiation (Fig. 2*F*).

The residues Gly^{417}, Val^{420}, and Ala^{421} share the same helix interface as the L*XX*FA*XX*L motif found in the NMR structure (*green* and *yellow*, respectively, in Fig. 2*G*). However, the resi-

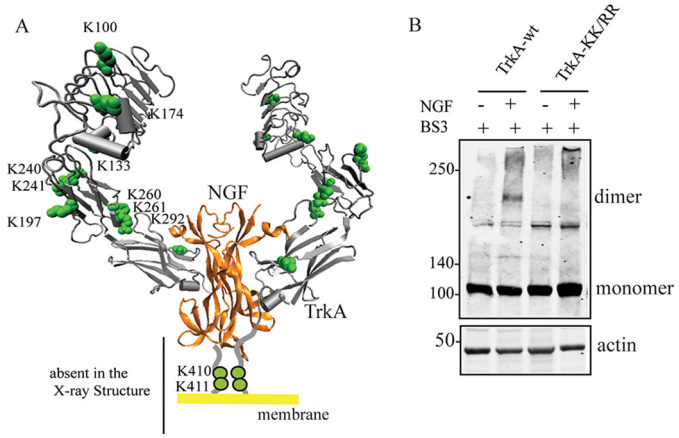

Figure 3. Lys^{410} and Lsy^{411} of eJTM are cross-linked with BS3 upon NGF binding. *A*, location of the Lys residues in the crystal structure of the rat TRKA-ECD/NGF complex (Protein Data Bank code 2IFG) (16). The Lys residues, shown in *green*, are located in the extracellular juxtamembrane region of the TRKA–ECD. *B*, Western immunoblots of lysates of HEK293 cells transfected with the indicated TRKA constructs (see Fig. 3*A*) and incubated with or without NGF in the presence the cross-linker BS3. Molecular weights are indicated at *left*. Actin was assayed as a loading control.

dues Val^{418} and Val^{422} are in a different interface. Interestingly the mutation V418C induces a ligand-independent differentiation of PC12nnr5 cells, indicating that this residue belongs to the active dimer interface (Fig. 2*G*).

The combined results of the functional assays suggest a transition from an inactive to an active dimer interface and support the importance of the NMR-derived TMD structure for TRKA activation. The residue Ala^{428} plays a critical role in TRKA activation by NGF. Its location in the closest dimer interface suggests a pivoting role in the transition from the ligand-free to the ligand-bound dimer interface (Fig. 2*G*). Because activation of TRKA is a consequence of this change in the dimer interface in the next sections, we study the nature of this conformational change induced by NGF binding.

NGF induces a rearrangement of the extracellular juxtamembrane region of TRKA

Stimulation of HeLa cells transfected with TRKA-wt with NGF induces the formation of TRKA dimers that are cross-linked with BS3 (Fig. 3). Although it has been described that TRKA dimers are formed in the absence of NGF, we were not able to detect cross-linking without the ligand, even at overexpression levels, supporting that NGF binding is not only promoting a TMD dimerization but is accompanied by changes in the conformation of the extracellular part of the protein. Because BS3 reacts only with free amines (the side chains of Lys residues or a free N terminus), we searched for possible sites in TRKA that might have caused the observed cross-linking. According to the crystal structure of the TRKA–NGF complex (15) (Fig. 3*A*), there are no lysine residues in the TRKA–ECD that are located in a position where cross-linking of the side chains of Lys residues of two monomers could occur. Because BS3 does not cross-the plasma membrane and because we used the full-length TRKA receptor in our assays, we wondered whether the observed BS3 cross-linking was mediated via cross-linking of Lys^{410} and Lys^{411} in the extracellular juxtamembrane region (eJTM) of TRKA (Fig. 3*A*) because this region is not observed in the crystal structure (16). To verify this hypothesis, we mutated both Lys^{410} and Lys^{411} to Arg and repeated the initial experiment using HEK293 cells transfected with this TRKA-KK/RR construct (Fig. 3*B*). No BS3-induced TRKA cross-linking was observed in the TRKA-KK/RR-transfected cells, suggesting that NGF binding brings this region of the eJTM into close proximity.

We considered that if NGF indeed induces contacts between these eJTM regions, then we should be able to mimic this activity of NGF by forcing the dimerization of eJTMs in the absence of NGF. For this purpose, we individually mutated most of the residues in the eJTM of TRKA to cysteine and subsequently analyzed the dimerization of these transfected single point mutants (Fig. 4*A*). After transfection of HeLa cells, disulfide dimers were spontaneously formed in all constructs but the amount of dimers differed between the various mutants (Fig. 4*B*). The amount of dimer is significantly higher in the positions D412C and K411C. As a functional assay, we then transfected these mutants into HeLa cells, which do not express endogenous TRKA and quantified the phosphorylation of the tyrosines from the kinase activation loop (Tyr$^{674/675}$) in the absence and presence of NGF (Fig. 4*C*). This analysis showed the presence of active dimers (D406C, K410C, and K411C) that are activated constitutively in the absence of NGF and dimers that are not active in the absence of NGF (V408C, D412C, E413C, and T414C). In the presence of NGF, these mutants showed no further activation by NGF (Fig. 4*C*), suggesting they are fully active and the dimer interface adopted by the cysteine dimers is similar or identical to the one obtained with NGF binding. As a whole, there is a poor correlation ($R^2 = 0.07$; Fig. 4*D*, *red line*) between the amount of dimer formation and constitutive activation, suggesting that dimerization by itself is not enough for TRKA activation. However. the mutants with higher constitutive activation (D406C, K410C, and K411C) showed a good correlation between dimer formation and activation ($R^2 = 0.92$; Fig. 4*D*, *green line*). We then transfected some of the active mutants in PC12nnr5 cells. In the absence of NGF, the R405C, K410C, and K411C mutants induced the formation of neurites in PC12nnr5 cells (Fig. 4, *F* and *G*), supporting the constitutive activation of these mutants and suggested that disulfide bond formation through this interface mimics the binding of NGF. If we assume that the TMD α-helix continues in the juxtamembrane region, the residues Asp^{406}, Lys^{410}, and Lys^{411} are in one face of the helix (in *green* in the Fig. 4*H*). By contrast the residues whose mutation to cysteine do not activate constitutively the receptor are located in another face (in *red* in Fig. 4*H*). All the mutants are correctly expressed at the plasma membrane as found by flow cytometry (Fig. 4*E*). In summary, our results support the notion of the insufficiency of TRKA dimerization alone for higher receptor activation and support the existence of a preferred active dimer interface that is formed upon ligand binding.

Insertion of leucine residues into the TMD constitutively activates TRKA

Overexpression of TRKA is able to activate the receptor in the absence of ligand, and as we show above, the TMD dimer interface is quite similar, although not identical, to the one

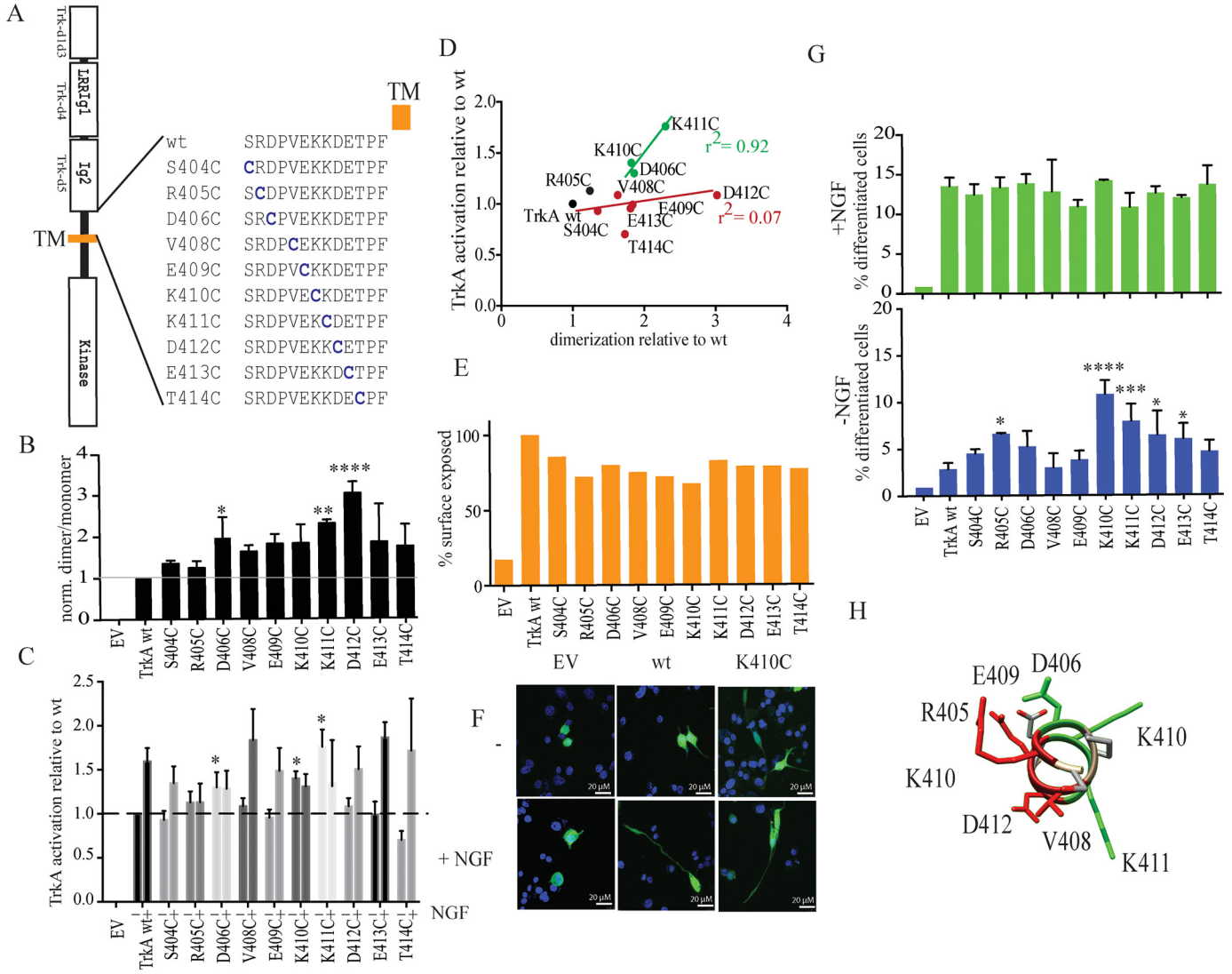

Figure 4. A preferred dimer interface in the TRKA juxtamembrane region. *A*, amino acid sequence of the rat TRKA cysteine mutant constructs that are mutated in the region of the eJTM closest to the TMD. *B*, quantification of the ratio of dimer:monomer of the TRKA mutants as determined using nonreducing SDS-PAGE. *C*, quantification of the activation of TRKA (with and without NGF) by quantifying the signal from the phosphorylation of the $Tyr^{674/675}$ signal using Western blotting of the cysteine mutants in the JTM region. *D*, scatter plot of the dimerization of TRKA cysteine mutants respect to its activation in the absence of NGF. A regression fit using the active (*green*) and inactive (*red*) cysteine mutant dimers is shown with the indicated r^2. *E*, cytometric analysis of the expression of the TRKA mutants at the plasma membrane of HeLa cells. *F*, PC12nnr5 cell differentiation assay of TRKA-wt and TRKA-K410C in the presence and absence of NGF. *G*, quantification of the differentiation of PC12nnr5 cells transfected with the indicated TRKA constructs and incubated in the absence (*blue bars*) or presence (*green bars*) of NGF. *H*, model of the eJTM into an ideal α-helix showing the spatial location of the indicted residues. *Error bars* represent the standard error of the mean. Statistics were done using two-way ANOVA and Dunnett's multiple comparison test using GraphPad software. The *p* values of significant differences are shown. ****, $p < 0.0001$. *EV*, empty vector.

obtained with NGF stimulation, suggesting that overexpression may induce a basal activation of TRKA. The Western blotting shown in Fig. 5*A* shows that although the overexpression of TRKA induces a ligand-independent activation, the presence of NGF is required for a higher and complete activation of the receptor. This could be the result of the conformational change induced by NGF binding in the JTM region concomitantly with the rotation of the dimer interface of the TMD dimer. This complete sequence of the events caused by the ligand is of great importance for receptor activation. To test this mechanism, we introduced a different number of leucine residues into the TRKA–TMD and analyzed the resulting TRKA activation in the absence of NGF (Fig. 5*B*). The insertion of each Leu should rotate the intracellular region around an angle of ~100°. Thus, Leu insertion allows evaluation of whether a change in the rotation angle of the intracellular domain plays any role in TRKA activation (Fig. 5*C*). We transfected the constructs TRKA-ins1L, TRKA-ins2L, TRKA-ins3L, and TRKA-ins4L that included 1–4 inserted leucines, respectively. The insertion of one Leu, TRKA-ins1Leu, significantly increased both the constitutive activation of TRKA in transfected HeLa cells compared with that of transfected TRKA-wt (Fig. 5, *D* and *E*) and the differentiation of PC12nnr5 cells compared with wt-transfected cells (Fig. 5*F*) in a ligand-independent manner. Equal levels of all constructs were expressed at the plasma membrane as determined using flow cytometry (Fig. S7). These data indicate that NGF binding is accompanied by a

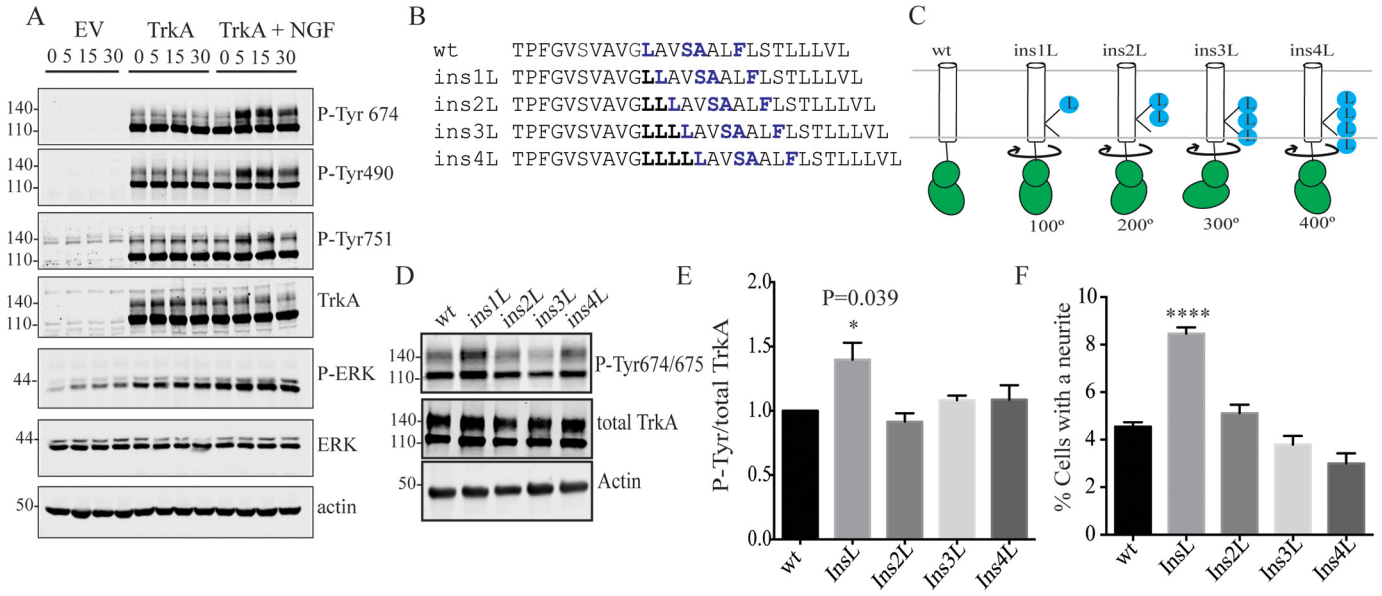

Figure 5. Rotation of the TRKA–TMD as a mechanism of TRKA activation by NGF. *A*, effect of NGF on the activation of overexpressed TRKA. HeLa cells transfected with the indicated constructs were stimulated with NGF (10 ng/ml) for 0, 5, 15, or 30 min. The immunoblots show the activation of TRKA as detected using an antibody specific for the autophosphorylated P-Tyr$^{674/675}$, P-Tyr^{490}, and P-Tyr^{751} residues and for the downstream activated P-ERK. The levels of total TRKA and total ERK are shown *below* each blot. Actin was blotted as a loading control. A representative blot of at least three independent experiments is shown. *B*, amino acid sequences of the rat TRKA Leu insertion mutants indicating the location of the inserted Leu residues. *C*, schematic drawing of the TRKA–TMD-ICD showing how the different numbers of inserted Leu residues (*blue*) in the TMD induce a different rotation of the intracellular domain (*green*). *D*, HeLa cells were transfected with the indicated TRKA–TMD insertion mutants. The immunoblots show the activation of TRKA as detected using an antibody specific for the TRKA autophosphorylation P-Tyr$^{674/675}$ residues. The levels of total TRKA are shown below. Actin was assayed as a loading control. *E*, quantification of the data in *D* from at least three independent experiments. *Bars* represent standard error of the mean. Statistical analysis was performed using one-way ANOVA with Dunnett's multicomparison test and TRKA-wt as a control. The *p* value of the significant difference is shown. *F*, PC12nnr5 cell differentiation of TRKA–TMD insertion mutant-transfected cells incubated in the absence of NGF. The percentage of the total GFP positive-transfected cells with a neurite twice as long as the length of the cell body was quantified. *Bars* represent the standard error of at least four independent experiments. Statistical analysis was performed using one-way ANOVA with Dunnett's multicomparison test and TRKA-wt as a control. The *p* values of significant differences are shown. *EV*, empty vector.

conformational rearrangement in the JTM that is transmitted, as a rotation of the TMD, to the intracellular region for TRKA activation.

Discussion

TRKA belongs to a subfamily of RTKs that includes the other family members TrkB and TrkC. These RTKs are essential for the formation of the nervous system and mediate a variety of cellular responses in normal biological processes and in pathological states (37). An understanding of their mechanism of action is necessary to facilitate the design of new pharmacological agents targeted to the processes in which they play a role.

In this regard, in the present work we posed two major questions: 1) what is the dimer interface of TRKA TMD in the active/inactive states? and 2) how is the coupling between the ligand binding and receptor activation? To answer the first question, we employed structural characterization using NMR spectroscopy together with mutagenesis studies, disulfide cross-linking, and functional assays. We described the high-resolution NMR structure of the TRKA transmembrane domain dimer, which is the first such description of a neurotrophin receptor of the Trk family. The obtained spatial structure was verified using functional assays and cross-linking, which confirmed both the relevance of this structure for TRKA activity and assignation of the found dimer conformation to the receptor active state. This result combined with the crystal structure of the extracellular domain of the TRKA complex with NGF (16, 38), the crystal structure of the TRKA inactive kinase domain (21, 22), and the recently reported structures of the entire TRKA intracellular region (39, 40) provides an almost complete picture of the full-length Trk receptor family, lacking only the structure of the small JTM regions. Our results highlight the key role of Ala^{428} in the activation of TRKA by NGF. The importance of this residue may reside in its pivotal position modulating the transition between the inactive to the active dimer interface. This transition could be hampered by the introduction of a bulky residue like Ile. This is also reflected by its high conservation in the TRKA and TrkC protein sequences from several species. The protein sequence divergence of TrkB–TMD is notable (Fig. 1) and may reflect a totally different mechanism of activation as has been recently proposed (41). The finding that the mutation of G423I reduces significantly the differentiation of PC12 cells with NGF suggests that small rearrangements in this TMD region could play an important role in the activation of the downstream signaling, leading to cell differentiation.

To answer the second question posed above, we investigated the role of the eJTM regions of the TRKA receptor upon NGF binding in receptor activation and dimerization. We showed that full-length TRKA receptors could be activated by specific single-point cysteine mutations in the eJTM and in the TMD, in which the position of the mutation relative to the TMD was more important for activation than the dimerization propensity of the mutant. In addition the insertion of Leu residues upstream of the TMD dimerization motif activated TRKA in

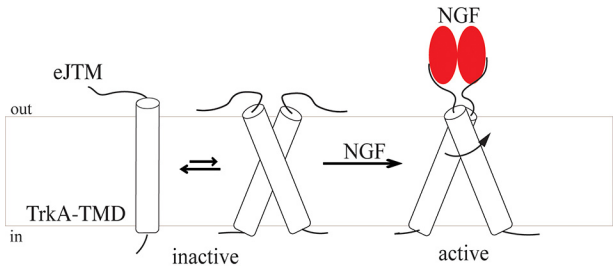

Figure 6. Model of the role of TRKA eJTM and TM domains in receptor activation. TRKA is in equilibrium monomer-dimer by TMD interactions. Binding of NGF stabilizes the TRKA dimers and induces a rearrangement of the eJTM that couples ligand binding to rotation of the TMD. For simplicity only the TMD plus the JTM region is shown. The NGF dimer is shown in *red*.

the absence of ligand. This suggests that rotation of the downstream domain may be behind the activation of the kinase domain. Other authors have suggested the rotational mechanism of RTK activation (42, 43). In this model the ligand would induce a rotation of the TMD dimer interface that will reorient the kinase domains to facilitate the transphosphorylation. Although our results support this model of activation, other alternative possibilities may exist. For instance the insertion of extra residues increases the TMD length and could induce a piston-like mechanism of activation. However, an increase in the length by two, three, or four residues should also activate the kinase, and this was not the case, because only the Ins1L mutant showed activation. Also, because the insertion of the residues are located into the TMD, it may alter the dimer interface of the TMD dimer, leading to the formation of another dimer interface compatible with a higher activation of the kinase domains. Although we cannot discard this possibility, in the constructs we made, the Leu residues were inserted upstream of the active dimer interface (Fig. 5*B*) to not alter the dimer interface found by NMR studies.

Bearing all of these findings in mind, we propose a mechanism of receptor activation that suggested a ligand-induced dimerization (or stabilization of preformed dimers) accompanied by a conformational change in the JTM that is transmitted to the intracellular regions by a rotation of the TMD (Fig. 6). This model is supported by our data showing that cysteine mutants in the eJTM and in the TMD in some specific positions can activate TRKA without ligand and that NGF binding induce the formation of new cysteine dimers in the TMD and the ligand-independent activation of TRKA by an induced rotation of its TMD. In addition our model may allow the existence of preformed inactive dimers of TRKA and a conformational activation by NGF as others have suggested (18, 44). Future structural and functional studies of the TRKA should address how the kinase domain is activated if they are connected to the TMD by a flexible intracellular juxtamembrane region. In summary, we have provided functional and structural evidence of the roles played by the JTM and the TMD in TRKA dimerization and activation by NGF.

Experimental procedures

DNA constructs

A plasmid encoding rat TRKA with an N-terminal hemagglutinin tag was kindly provided by Dr. Y. Barde. All TRKA mutants and constructs were derived from this plasmid. Mutagenesis was done using the site-directed mutagenesis kit (Agilent) according to the manufacturer's protocol. The oligonucleotide sequences of all of the constructs are available upon request. All DNA constructs were sequenced using local facilities.

Cell culture and transfection

HeLa cells, which do not express endogenous TRKA, were cultured in Dulbecco's modified Eagle's medium (Fisher) supplemented with 10% fetal bovine serum (Fisher) at 37 °C in a humidified atmosphere with 5% CO_2. PC12 and PC12nnr5 cells were cultured in Dulbecco's modified Eagle's medium with 10% fetal bovine serum and 5% horse serum (Fisher). Transfection of HeLa cells was performed using polyethylenimine (PEI; Sigma) at a concentration of 1–2 μg/μl. The use of PEI as the transfection reagent for HeLa cells resulted in suboptimal transfection (10–15% of cells transfected) and in the expression of only a small amount of TRKA in the cells. In contrast, when the same PEI/DNA ratio was used for transfection of HEK293 cells, TRKA was expressed in higher amounts, and ligand-independent activation of TRKA was seen. A concentration of 500–1000 ng of DNA per 10-cm cell plate was used for the TRKA activation experiments. Twenty-four hours after transfection, the cells were lifted and replated into 12-well plates at a density of 100,000 cells/well. By using this procedure, the percentage of cells transfected was identical in all the wells. Forty-eight hours after transfection, the cells were starved in serum-free medium for 2 h and were then stimulated with NGF (Alomone) at the indicated concentrations and time intervals. The cells were lysed with TNE buffer (Tris-HCl, pH 7.5, 150 mM NaCl, 1 mM EDTA) supplemented with 1% Triton X-100 (Sigma), protease inhibitors (Roche), 1 mM phenylmethylsulfonyl fluoride (Sigma), 1 mM sodium orthovanadate (Sigma), and 1 mM sodium fluoride (Sigma). In the experiments involving the TRKA cysteine mutants, 10 mM iodoacetamide (Sigma) was added to the lysis buffer. Lysates were kept on ice for 10 min and centrifuged at 12,000 × *g* for 15 min in a tabletop centrifuge. The protein level of the lysates was quantified using a Bradford kit (Pierce), and lysates were analyzed by SDS-PAGE

Western blotting analysis

Cellular debris was removed by centrifugation at 12,000 × *g* for 15 min, and the protein level of cell lysates was quantified using the Bradford assay (Pierce). The proteins were resolved in SDS-PAGE gels and transferred to nitrocellulose membranes that were incubated overnight at 4 °C with one of the following antibodies: mouse monoclonal anti-hemagglutinin (1:2000, Sigma); rabbit polyclonal MBP-probe (1:1000, Santa Cruz); rabbit anti-P-Tyr$^{674/675}$ (1:1000, Cell Signaling); and rabbit anti-TRKA (1:1000, Millipore). Following incubation with the appropriate secondary antibody, the membranes were imaged, and the bands were quantified using enhanced chemiluminescence and autoradiography.

TRKA–TMD constructs for cell-free expression

The gene encoding the transmembrane domain of the human TRKA-TM (^{409}MKKDETPFGVSVAVGLAVFACLFL-

STLLLVLNKAGRRNK[447]) was amplified by PCR from six chemically synthesized oligonucleotide templates (Evrogen) whose sequences partially overlapped along its sequence. The PCR products were cloned into a pGEMEX-1 vector by three-component ligation using the NdeI, AatII, and BamHI restriction sites.

Cell-free gene expression

A bacterial S30 cell-free extract was prepared from a 10-liter culture of the *Escherichia coli* Rosetta(DE3)pLysS strain according to a previously described protocol. The S30 cell extract was stored in 500-μl aliquots at −80 °C. The continuous exchange mode of preparation using a 12.5-kDa membrane was used in this study. Preparative-scale reactions (2–3 ml of reaction mixture) were carried out in 50-ml tubes. Optimal reaction conditions such as Mg^{2+} and K^{+} concentrations, the ratio of the reaction mixture to the feeding mixture or the DNA concentration were established using homemade reactors based on the Mini-CECF reactor previously described (45, 46). The final reaction mixture was a standard feeding mixture:reaction mixture ratio of 8:1 and a cell-free reaction mixture containing 100 mM HEPES, 0.83 mM EDTA with KOH added to achieve a pH of 8.0, 0.1 mg/ml folinic acid, 20 mM acetyl phosphate, 1.2 mM ATP, 0.8 mM each of G/C/UTP, 2 mM 1,4-DTT, 0.05% sodium azide, 2% PEG 8000, 20 mM magnesium acetate, 270 mM potassium acetate, 60 mM creatine phosphate, 1 mM each of 20 amino acids or 0.25% of a 20-amino acid mix (Cambridge Isotope Laboratories, USA), 1 tablet/50 ml of complete protease inhibitor (Roche, Switzerland), 0.5 mg/ml *E. coli* tRNA (Roche, Switzerland), 0.25 mg/ml creatine kinase from rabbit muscle (Roche, Switzerland), 0.05 mg/ml T7 RNA polymerase prepared using a previously described protocol (47), 0.1 unit/μl Ribolock (Fermentas), 0.02 μg/μl plasmid DNA, and 30% S30 cell-free extract. All reagents were provided by Sigma unless otherwise specified. Plasmid DNA was purified using a Promega MaxiPrep kit. The reactions were conducted overnight at 34 °C and in an Innova 44R shaker (New Brunswick) set at 150 rpm.

Protein purification

The cell-free reaction mixture was diluted three-times with buffer A (50 mM Tris, pH 8.0, and 200 mM NaCl). After 10 min of incubation, the mixture was centrifuged for 10 min at 18,000 × *g* at room temperature. The precipitate was washed consecutively with buffer A containing 30 μg/ml RNase A (Fermentas) and buffer B (50 mM Tris, pH 8.0, and 100 mM NaCl). The target protein was solubilized with 200 μl of buffer B containing 1% lauryl sarcosine. After each step, the protein was centrifuged for 10 min at 18,000 × *g* at room temperature, and aliquots of the supernatant were analyzed using 12.5% Tricine SDS-PAGE (53). The clarified protein solution was applied onto a 10/300 Tricorn column prepacked with Superdex 200 (GE Healthcare) and pre-equilibrated with buffer B containing 0.2% lauryl sarcosine. Protein-containing fractions were combined and precipitated using the TCA/acetone procedure (48).

Preparation of NMR samples in a membrane mimetic medium

The so-called "isotopic heterodimer" (1:1 mixture of unlabeled and $^{15}N/^{13}C$-labeled peptides) samples were prepared corresponding to the TRKA–TMD construct to solve its structure. The powder containing the peptides of both samples was first dissolved in a 1:1 trifluoroethanol–H_2O mixture with the addition of deuterated DPC (d_{38}, 98%, Cambridge Isotope Laboratories, USA) and phosphate buffer and was then kept for several minutes in an ultrasound bath and lyophilized. Subsequently, the dried samples were dissolved in 350 μl of a 9:1 H_2O:D_2O mixture. To attain a uniform micelle size and uniform distribution of the peptide throughout the micelles, the samples were sonicated in an ultrasound bath for several minutes until the solution was completely transparent. The TRKA–TMD concentration in the isotopic-heterodimer sample was 1.9 mM, and other conditions were as follows: DPR 50:1, pH 5.9, and 20 mM phosphate buffer. The samples were placed in Shigemi NMR tubes with a glass plunger. Selective-residue labeling was implemented to avoid peaks overlapping while processing the NMR spectra.

NMR spectroscopy and spatial structure calculation

NMR spectra were acquired at 45 °C using 600 and 800 MHz AVANCE III spectrometers (Bruker BioSpin, Germany) equipped with pulsed-field gradient triple-resonance cryoprobes. ^{1}H, ^{13}C, and ^{15}N resonances of TRKA–TMD were assigned with CARA software (49) using two- and three-dimensional heteronuclear experiments (50): $^{1}H/^{15}N$ HSQC, $^{1}H/^{15}N$ transverse relaxation optimised spectroscopy, $^{1}H/^{13}C$ HSQC, $^{1}H/^{15}N$ HNHA, $^{1}H/^{13}C/^{15}N$ HNCA, $^{1}H/^{13}C/^{15}N$ HN(CO)CA, $^{1}H/^{13}C/^{15}N$ HNCO, 3D-HccH total correlation spectroscopy, and ^{13}C- and ^{15}N-edited NOESY HSQC (recorded on 600 and 800 MHz spectrometers, respectively). Dimeric spatial structures were calculated with the CYANA program (51) based on torsion angle restraints estimated from the chemical shift values obtained with the standard protocol of the TALOS-N program (52) and with intra- and intermonomeric NOE distance restraints derived through analysis of the three-dimensional ^{15}N- and ^{13}C-edited NOESY and ^{15}N,^{13}C F1-filtered/F3-editedNOESY spectra (50) acquired for isotopic heterodimer samples. MOLMOL software was used to calculate the contact areas between the dimer subunits and to visualize the structures (53). Hydrophobic properties of the α-helices in the TRKA–TMD dimers were calculated using the molecular hydrophobicity potential approach implemented in the PREDDIMER program (54).

Free energy measurements

To measure the free energy we used an NMR-based approach (31). 1 mM ^{15}N-labeled TRKA–TMD sample was prepared in DPC micelles at DPR 50 in NMR buffer and then bxgradually diluted by 10% DPC solution. At each point, the band-selective excitation short transient-transverse relaxation optimised spectroscopy spectrum with a 0.8-s relaxation delay was acquired to ensure the equilibrium longitudinal magnetization of amide protons (55). The populations of monomeric, dimeric, and oligomeric states were measured from the integrals of separate cross-peaks in these spectra, applying the correction to take into account the coherence losses caused by the transverse relaxation (31). Obtained populations were then converted to monomer and dimer concentrations and approx-

imated by the micelle-based model of TMD dimerization (31): $K_D = M^2/(D[\text{Emic}])$, where M and D stand for the concentrations of monomer and dimer, whereas [Emic] is the concentration of "empty" micelles. An additional constraint equation was applied: $N_e[\text{Emic}] + N_m M + N_d D = [\text{Dpc}]$, where N_e, N_m, and N_d stand for the number in detergent molecules in empty, monomer-bearing, and dimer-bearing micelles, respectively. N_e was fixed to 55 (56), whereas K_D, N_m, and N_d were the parameters of approximation. The resulting free energy was additionally corrected by $RT\ln(N_e)$, to change to the generally accepted standard conditions of 1 M detergent (the original value corresponded to the standard conditions of 1 M of empty micelles) (57).

Isolation of membrane fractions

TRKA mutants were overexpressed in HeLa cells by transfection using PEI (1 mg/ml; Sigma). 48 h after transfection, the cells were resuspended in 1 ml of ice-cold homogenization buffer (250 mM sucrose, 1 mM EDTA, 10 mM Tris buffer, pH 7.1, plus protease inhibitors) and broken by sonication in two time intervals (30 and 30 s) with 50 W and frequency at 30 MHz on ice. The broken cell homogenate was centrifuged for 10 min at 500 × *g* at 4 °C to remove whole cells and nuclei. To collect the membrane fraction the cleared supernatant was centrifuged at 100,000 × *g* at 4 °C for 1 h in a Beckman Optima MAX ultracentrifuge with a TLA110 rotor using polycarbonate thick-wall centrifuge tubes (Beckman Coulter). The supernatant that contains soluble proteins was removed, and the pellet-containing membranes were resuspended in 1 ml of ice-cold homogenization buffer by sonication and recentrifuged at 100,000 × *g*. The final pellet contains the membrane fraction used to the iodine oxidation protocol.

Iodine oxidation for cross-linking of TRKA mutants

Because cysteine residues are buried deep in the phospholipid bilayer, the membranes were isolated, and I_2 was used as the oxidation agent as described in Ref. 58. The membrane fractions were diluted in the homogenization buffer (250 mM sucrose, 1 mM EDTA, 10 mM Tris buffer, pH 7.1 plus protease inhibitors). Protein content was quantified using a Bradford kit (Pierce), and equal amounts of isolated membranes fractions were incubated for 10 min with or without NGF (10 ng/ml). A solution of 2.5 mM I_2 in absolute ethanol was freshly prepared immediately before the cross-linking of cysteine residues and was added to the incubated membrane fractions with NGF (250 μM final iodine concentration) for 30 s at room temperature. The reaction was stop adding 1/10 volume of a freshly made solution of sodium thiosulfate (60 μM final concentration). Nonreducing SDS-PAGE sample buffer was added, and the samples were boiled for 5 min before analyzed by nonreducing SDS-PAGE.

Differentiation of PC12nnr5 cells

Transfection in PC12nnr5 cells was performed using Lipofectamine 2000 as per the manufacturer's instructions. The mutant or the WT TRKA-transfected cells and mock-transfected cells, as well as nontransfected cells, were treated under the same conditions in a 6-well tissue culture plate. The cells were washed three times with serum-free medium and incubated for 48 h in a medium containing 1% fetal bovine serum and 50 ng/ml of NGF (Alomone). At time 0, 24 h, and 48 h, the cells were washed with cold PBS and fixed with 4% paraformaldehyde for 15 min at room temperature. The cells were imaged using a Leica SP8 spectral confocal microscope. The percentage of cells with a neurite twice as long as the cell body was counted as differentiated.

Accession codes

The atomic coordinates and experimental restraints were deposited in the Protein Data Bank under accession code 2n90 for TRKA-TM-wt.

Author contributions—M. L. F., S. A. G., K. S. M., A. S. A., and M. V. conceptualization; M. L. F. and M. V. data curation; M. L. F., K. D. N., S. A. G., K. S. M., A. S. A., and M. V. formal analysis; M. L. F. and M. V. supervision; M. L. F., A. S. A., and M. V. funding acquisition; M. L. F., K. D. N., S. A. G., K. S. M., A. S. A., and M. V. investigation; M. L. F., K. D. N., S. A. G., K. S. M., A. S. A., and M. V. methodology; M. L. F. and M. V. writing-original draft; M. L. F., S. A. G., K. S. M., A. S. A., and M. V. writing-review and editing.

Acknowledgments—We thank Dr. Carlos Ibañez for critical reading of the manuscript and Dr. Yves Barde for the TRKA plasmid.

References

1. Chao, M. V. (2003) Neurotrophins and their receptors: a convergence point for many signalling pathways. *Nat. Rev. Neurosci.* **4,** 299–309 CrossRef Medline
2. Bothwell, M. (2014) NGF, BDNF, NT3, and NT4. *Handb. Exp. Pharmacol.* **220,** 3–15 CrossRef Medline
3. Ceni, C., Unsain, N., Zeinieh, M. P., and Barker, P. A. (2014) Neurotrophins in the regulation of cellular survival and death. *Handb. Exp. Pharmacol.* **220,** 193–221 CrossRef Medline
4. Friedman, W. J., and Greene, L. A. (1999) Neurotrophin signaling via Trks and p75. *Exp. Cell Res.* **253,** 131–142 CrossRef Medline
5. Bothwell, M. (2016) Recent advances in understanding neurotrophin signaling. *F1000Research* **5,** 1885 CrossRef Medline
6. Vilar, M. (2017) Structural characterization of the p75 neurotrophin receptor: a stranger in the TNFR superfamily. *Vitam. Horm.* **104,** 57–87 CrossRef Medline
7. Smeyne, R. J., Klein, R., Schnapp, A., Long, L. K., Bryant, S., Lewin, A., Lira, S. A., and Barbacid, M. (1994) Severe sensory and sympathetic neuropathies in mice carrying a disrupted Trk/NGF receptor gene. *Nature* **368,** 246–249 CrossRef Medline
8. Indo, Y., Tsuruta, M., Hayashida, Y., Karim, M. A., Ohta, K., Kawano, T., Mitsubuchi, H., Tonoki, H., Awaya, Y., and Matsuda, I. (1996) Mutations in the TRKA–NGF receptor gene in patients with congenital insensitivity to pain with anhidrosis. *Nat. Genet.* **13,** 485–488 CrossRef Medline
9. Martin-Zanca, D., Hughes, S. H., and Barbacid, M. (1986) A human oncogene formed by the fusion of truncated tropomyosin and protein tyrosine kinase sequences. *Nature* **319,** 743–748 CrossRef Medline
10. Cocco, E., Scaltriti, M., and Drilon, A. (2018) NTRK fusion-positive cancers and TRK inhibitor therapy. *Nat. Rev. Clin. Oncol.* **15,** 731–747 CrossRef Medline
11. Endres, N. F., Barros, T., Cantor, A. J., and Kuriyan, J. (2014) Emerging concepts in the regulation of the EGF receptor and other receptor tyrosine kinases. *Trends Biochem. Sci.* **39,** 437–446 CrossRef Medline
12. Lemmon, M. A., and Schlessinger, J. (2010) Cell signaling by receptor tyrosine kinases. *Cell* **141,** 1117–1134 CrossRef Medline
13. Wiesmann, C., Ultsch, M. H., Bass, S. H., and de Vos, A. M. (1999) Crystal structure of nerve growth factor in complex with the ligand-binding domain of the TRKA receptor. *Nature* **401,** 184–188 CrossRef Medline

14. Arevalo, J. C., Conde, B., Hempstead, B. I., Chao, M. V., Martín-Zanca, D., and Pérez, P. (2001) A novel mutation within the extracellular domain of TRKA causes constitutive receptor activation. *Oncogene* **20,** 1229–1234 CrossRef Medline
15. Zaccaro, M. C., Ivanisevic, L., Perez, P., Meakin, S. O., and Saragovi, H. U. (2001) p75 Co-receptors regulate ligand-dependent and ligand-independent Trk receptor activation, in part by altering Trk docking subdomains. *J. Biol. Chem.* **276,** 31023–31029 CrossRef Medline
16. Wehrman, T., He, X., Raab, B., Dukipatti, A., Blau, H., and Garcia, K. C. (2007) Structural and mechanistic insights into nerve growth factor interactions with the TRKA and p75 receptors. *Neuron* **53,** 25–38 CrossRef Medline
17. Mischel, P. S., Umbach, J. A., Eskandari, S., Smith, S. G., Gundersen, C. B., and Zampighi, G. A. (2002) Nerve growth factor signals via preexisting TRKA receptor oligomers. *Biophys. J.* **83,** 968–976 CrossRef Medline
18. Shen, J., and Maruyama, I. N. (2011) Nerve growth factor receptor TRKA exists as a preformed, yet inactive, dimer in living cells. *FEBS Lett.* **585,** 295–299 CrossRef Medline
19. Marchetti, L., Callegari, A., Luin, S., Signore, G., Viegi, A., Beltram, F., and Cattaneo, A. (2013) Ligand signature in the membrane dynamics of single TRKA receptor molecules. *J. Cell Sci.* **126,** 4445–4456 CrossRef Medline
20. Ahmed, F., and Hristova, K. (2018) Dimerization of the Trk receptors in the plasma membrane: effects of their cognate ligands. *Biochem. J.* **475,** 3669–3685 CrossRef Medline
21. Artim, S. C., Mendrola, J. M., and Lemmon, M. A. (2012) Assessing the range of kinase autoinhibition mechanisms in the insulin receptor family. *Biochem. J.* **448,** 213–220 CrossRef Medline
22. Bertrand, T., Kothe, M., Liu, J., Dupuy, A., Rak, A., Berne, P. F., Davis, S., Gladysheva, T., Valtre, C., Crenne, J. Y., and Mathieu, M. (2012) The crystal structures of TRKA and TrkB suggest key regions for achieving selective inhibition. *J. Mol. Biol.* **423,** 439–453 CrossRef Medline
23. Bocharov, E. V., Bragin, P. E., Pavlov, K. V., Bocharova, O. V., Mineev, K. S., Polyansky, A. A., Volynsky, P. E., Efremov, R. G., and Arseniev, A. S. (2017) The conformation of the epidermal growth factor receptor transmembrane domain dimer dynamically adapts to the local membrane environment. *Biochemistry* **56,** 1697–1705 CrossRef Medline
24. Li, E., and Hristova, K. (2006) Role of receptor tyrosine kinase transmembrane domains in cell signaling and human pathologies. *Biochemistry* **45,** 6241–6251 CrossRef Medline
25. Li, E., and Hristova, K. (2010) Receptor tyrosine kinase transmembrane domains: function, dimer structure and dimerization energetics. *Cell Adhesion Migration* **4,** 249–254 CrossRef Medline
26. Jura, N., Endres, N. F., Engel, K., Deindl, S., Das, R., Lamers, M. H., Wemmer, D. E., Zhang, X., and Kuriyan, J. (2009) Mechanism for activation of the EGF receptor catalytic domain by the juxtamembrane segment. *Cell* **137,** 1293–1307 CrossRef Medline
27. King, C., and Hristova, K. (2019) Direct measurements of VEGF·VEGFR2 binding affinities reveal the coupling between ligand binding and receptor dimerization. *J. Biol. Chem.* **294,** 9064–9075 CrossRef Medline
28. Sarabipour, S., Ballmer-Hofer, K., and Hristova, K. (2016) VEGFR-2 conformational switch in response to ligand binding. *eLife* **5,** e13876 CrossRef Medline
29. Sarabipour, S., and Hristova, K. (2016) Mechanism of FGF receptor dimerization and activation. *Nat. Commun.* **7,** 10262 CrossRef Medline
30. Nadezhdin, K. D., García-Carpio, I., Goncharuk, S. A., Mineev, K. S., Arseniev, A. S., and Vilar, M. (2016) Structural Basis of p75 Transmembrane Domain Dimerization. *J. Biol. Chem.* **291,** 12346–12357 CrossRef Medline
31. Mineev, K. S., Lesovoy, D. M., Usmanova, D. R., Goncharuk, S. A., Shulepko, M. A., Lyukmanova, E. N., Kirpichnikov, M. P., Bocharov, E. V., and Arseniev, A. S. (2014) NMR-based approach to measure the free energy of transmembrane helix-helix interactions. *Biochim. Biophys. Acta* **1838,** 164–172 CrossRef Medline
32. Mineev, K. S., Goncharuk, S. A., and Arseniev, A. S. (2014) Toll-like receptor 3 transmembrane domain is able to perform various homotypic interactions: an NMR structural study. *FEBS Lett.* **588,** 3802–3807 CrossRef Medline
33. Bocharov, E. V., Mineev, K. S., Goncharuk, M. V., and Arseniev, A. S. (2012) Structural and thermodynamic insight into the process of "weak" dimerization of the ErbB4 transmembrane domain by solution NMR. *Biochim. Biophys. Acta* **1818,** 2158–2170 CrossRef Medline
34. Cymer, F., Veerappan, A., and Schneider, D. (2012) Transmembrane helix-helix interactions are modulated by the sequence context and by lipid bilayer properties. *Biochim. Biophys. Acta* **1818,** 963–973 CrossRef Medline
35. Hughson, A. G., Lee, G. F., and Hazelbauer, G. L. (1997) Analysis of protein structure in intact cells: crosslinking *in vivo* between introduced cysteines in the transmembrane domain of a bacterial chemoreceptor. *Protein Sci.* **6,** 315–322 Medline
36. Schecterson, L. C., Hudson, M. P., Ko, M., Philippidou, P., Akmentin, W., Wiley, J., Rosenblum, E., Chao, M. V., Halegoua, S., and Bothwell, M. (2010) Trk activation in the secretory pathway promotes Golgi fragmentation. *Mol. Cell Neurosci.* **43,** 403–413 CrossRef Medline
37. Deinhardt, K., and Chao, M. V. (2014) Trk receptors. *Handb. Exp. Pharmacol.* **220,** 103–119 CrossRef Medline
38. Ultsch, M. H., Wiesmann, C., Simmons, L. C., Henrich, J., Yang, M., Reilly, D., Bass, S. H., and de Vos, A. M. (1999) Crystal structures of the neurotrophin-binding domain of TRKA, TrkB and TrkC. *J. Mol. Biol.* **290,** 149–159 CrossRef Medline
39. Furuya, N., Momose, T., Katsuno, K., Fushimi, N., Muranaka, H., Handa, C., Ozawa, T., and Kinoshita, T. (2017) The juxtamembrane region of TRKA kinase is critical for inhibitor selectivity. *Bioorg. Med. Chem. Lett.* **27,** 1233–1236 CrossRef Medline
40. Su, H. P., Rickert, K., Burlein, C., Narayan, K., Bukhtiyarova, M., Hurzy, D. M., Stump, C. A., Zhang, X., Reid, J., Krasowska-Zoladek, A., Tummala, S., Shipman, J. M., Kornienko, M., Lemaire, P. A., Krosky, D., *et al.* (2017) Structural characterization of nonactive site, TRKA-selective kinase inhibitors. *Proc. Natl. Acad. Sci. U.S.A.* **114,** E297–E306 CrossRef Medline
41. Zahavi, E. E., Steinberg, N., Altman, T., Chein, M., Joshi, Y., Gradus-Pery, T., and Perlson, E. (2018) The receptor tyrosine kinase TrkB signals without dimerization at the plasma membrane. *Sci. Signal.* **11,** eaao4006 CrossRef Medline
42. Bell, C. A., Tynan, J. A., Hart, K. C., Meyer, A. N., Robertson, S. C., and Donoghue, D. J. (2000) Rotational coupling of the transmembrane and kinase domains of the Neu receptor tyrosine kinase. *Mol. Biol. Cell* **11,** 3589–3599 CrossRef Medline
43. Maruyama, I. N. (2015) Activation of transmembrane cell-surface receptors via a common mechanism?: The "rotation model." *Bioessays* **37,** 959–967 Medline
44. Shen, J., and Maruyama, I. N. (2012) Brain-derived neurotrophic factor receptor TrkB exists as a preformed dimer in living cells. *J. Mol. Signal.* **7,** 2 CrossRef Medline
45. Aoki, M., Matsuda, T., Tomo, Y., Miyata, Y., Inoue, M., Kigawa, T., and Yokoyama, S. (2009) Automated system for high-throughput protein production using the dialysis cell-free method. *Protein Expr. Purif.* **68,** 128–136 CrossRef Medline
46. Kai, L., Roos, C., Haberstock, S., Proverbio, D., Ma, Y., Junge, F., Karbyshev, M., Dötsch, V., and Bernhard, F. (2012) Systems for the cell-free synthesis of proteins. *Methods Mol. Biol.* **800,** 201–225 CrossRef Medline
47. Schwarz, D., Junge, F., Durst, F., Frölich, N., Schneider, B., Reckel, S., Sobhanifar, S., Dötsch, V., and Bernhard, F. (2007) Preparative scale expression of membrane proteins in *Escherichia coli*-based continuous exchange cell-free systems. *Nat. Protoc.* **2,** 2945–2957 CrossRef Medline
48. Goncharuk, S. A., Goncharuk, M. V., Mayzel, M. L., Lesovoy, D. M., Chupin, V. V., Bocharov, E. V., Arseniev, A. S., and Kirpichnikov, M. P. (2011) Bacterial synthesis and purification of normal and mutant forms of human FGFR3 transmembrane segment. *Acta Naturae* **3,** 77–84 Medline
49. Keller, R. L. J. (2004) *The Computer Aided Resonance Assignment Tutorial*, Cantina Verlag, Goldau, Switzerland

50. Cavanagh, J., Fairbrother, W. J., Palmer, A. G., and Skelton, N. J. (2006) *Protein NMR Spectroscopy: Principles and Practice*, 2nd ed., Academic Press, San Diego, CA
51. Güntert, P. (2003) Automated NMR protein structure calculation. *Prog. NMR Spectrosc.* **43,** 105 CrossRef
52. Shen, Y., and Bax, A. (2013) Protein backbone and sidechain torsion angles predicted from NMR chemical shifts using artificial neural networks. *J. Biomol. NMR* **56,** 227–241 CrossRef Medline
53. Koradi, R., Billeter, M., and Wüthrich, K. (1996) MOLMOL: a program for display and analysis of macromolecular structures. *J. Mol. Graph.* **14,** 51–55, 29–32 CrossRef Medline
54. Polyansky, A. A., Volynsky, P. E., and Efremov, R. G. (2012) Multistate organization of transmembrane helical protein dimers governed by the host membrane. *J. Am. Chem. Soc.* **134,** 14390–14400 CrossRef Medline
55. Favier, A., and Brutscher, B. (2011) Recovering lost magnetization: polarization enhancement in biomolecular NMR. *J. Biomol. NMR* **49,** 9–15 CrossRef Medline
56. Tieleman, D. P., van der Spoel, D., and Berendsen, H. J. C. (2000) Molecular dynamics simulations of dodecylphosphocholine micelles at three different aggregate sizes: micellar structure and chain relaxation. *J. Phys. Chem. B* **104,** 6380–6388 CrossRef
57. Fleming, K. G. (2002) Standardizing the free energy change of transmembrane helix-helix interactions. *J. Mol. Biol.* **323,** 563–571 CrossRef Medline
58. Schwem, B. E., and Fillingame, R. H. (2006) Cross-linking between helices within subunit a of *Escherichia coli* ATP synthase defines the transmembrane packing of a four-helix bundle. *J. Biol. Chem.* **281,** 37861–37867 CrossRef Medline

Structural basis of the transmembrane domain dimerization and rotation in the activation mechanism of the TRKA receptor by nerve growth factor

María L. Franco, Kirill D. Nadezhdin, Sergey A. Goncharuk, Konstantin S. Mineev, Alexander S. Arseniev and Marçal Vilar

J. Biol. Chem. 2020, 295:275-286.
doi: 10.1074/jbc.RA119.011312 originally published online December 4, 2019

Supplemental Figure Legends

Figure S1. Dimerization of the TrkA-TMD in micelles.

(A) Percentage of the monomeric (green), dimeric (blue) and oligomeric (red) forms of the human TrkA-TMD at different LPRs. Population values were calculated from the cross-peak intensities in the $^{1}H/^{15}N$-TROSY-HSQC spectra.

(B) Apparent free energy of dimerization of the TrkA-TMD ($\Delta Gapp$)=RTln([M]2/[D]) plotted as a function of RTln(X), where X = ([Det]−Nm[M]−Nd[D])/Ne. [M], [D] and [Det] represent monomer, dimer and DPC concentration, respectively. Ne represents the number of DPC molecules per empty micelle, and Nm and Nd represent the number of DPC molecules per micelle for monomers and dimers, respectively.

Figure S2. Summary of the NMR data for the TrkA-TMD embedded into DPC micelles.

A) NOE connectivities observed in the $^{1}H/^{15}N$-NOESY-HSQC spectrum for the TrkA-TMD peptide.

B) Secondary $^{13}C\alpha$ chemical shifts of the TrkA-TMD are given by the difference between the actual chemical shift and a typical random-coil chemical shift for a specific residue. Pronounced positive or negative $\Delta\delta(^{13}C\alpha)h–c$ values indicate a helical structure or an extended conformation of a protein.

C) Local rotation correlation times t_R (ns) values of the amide groups derived from ^{15}N-relaxation data. Decreased t_R values indicate enhanced local flexibility of the protein backbone.

Figure S3. Assessment of the quality of the NMR-derived TrkA-TMD dimer structure. Structural alignment of the 10 lowest energy NMR structures of TrkA- TMD dimers.

Figure S4. Hydrophobicity map of the TrkA-TMD dimer.

The black oval delineates an helix-packing interface as calculated with the PREDIMER software. The residues within this black oval comprise the TrkA-TMD dimerization interface. The panels to the right show the percentage of inter-monomer contact surface

area.

Figure S5. TrkA-concentration-dependence of ligand-independent activation of TrkA. Increasing amounts of TrkA were transfected into Hela cells using PEI. After 48 h, the cells were stimulated or not with NGF (10 ng/mL). Cell lysates were analyzed by SDS-PAGE immnoblotting using antibodies specific for TrkA phospho- Tyr674/675 and total TrkA.

Figure S6. Membrane localization of TrkA mutants in Hela cells. Confocal fluorescence images of Hela cells transiently transfected with the indicated TrkA constructs. The cells were fixed and analyzed using an antibody against HA located in the N-terminus of TrkA, which was detected with a secondary antibody conjugated with the fluorophore alexa-555 (Red). Blue, nuclear DAPI staining. The cells shown are representative of 10 transfected cells analyzed for each condition.

Figure S7. Membrane localization of TrkA mutants in Hela cells by cytometric analysis. Percentage of TrkA constructs expressed at the plasma membrane relative to TrkA-wt (100%) obtained in Hela cells transfected with the indicated constructs and analyzed by flow cytometry using an HA primary antibody and a secondary antibody labeled with a fluorophore for alexa-488. EV is empty vector.

Figure 1- Table supplement 1

NMR distance & dihedral restraints	
Total unambiguous NOE restraints	360
intra-residue	136
inter-residue	228
sequential (|i-j|=1)	138
medium-range (1<|i-j|≤4)	76
long-range (|i-j|>4)	0
inter-monomeric NOE	16
Hydrogen bond restraints (upper/lower)	144/144
Total torsion angle restraints	118
backbone φ	52
backbone ψ	51
side-chain χ^1	15

Structure calculation statistics	
CYANA target function (Å^2)	0.64±0.21
Average pairwise r.m.s.d. (Å)	
TM α-helical region	
backbone atoms	0.18±0.07
all heavy atoms	0.36±0.07
Ramachandran analysis [a]	
% residues in most favoured regions	90.6
% residues in additional allowed regions	9.4
% residues in generously allowed regions	0.0
% residues in disallowed regions	0.0
Helix-helix packing	
Contact surface area per dimer subunit (Å^2)	370±40
Angle θ between the helix axes (deg.)	40±5
Distance d between the helix axes (Å)	
TM region	8.8±0.5

Table note:
[a] Ramachandran statistics was determined using CYANA
[b] Residues from unfolded and flexible regions

Figure S1

A

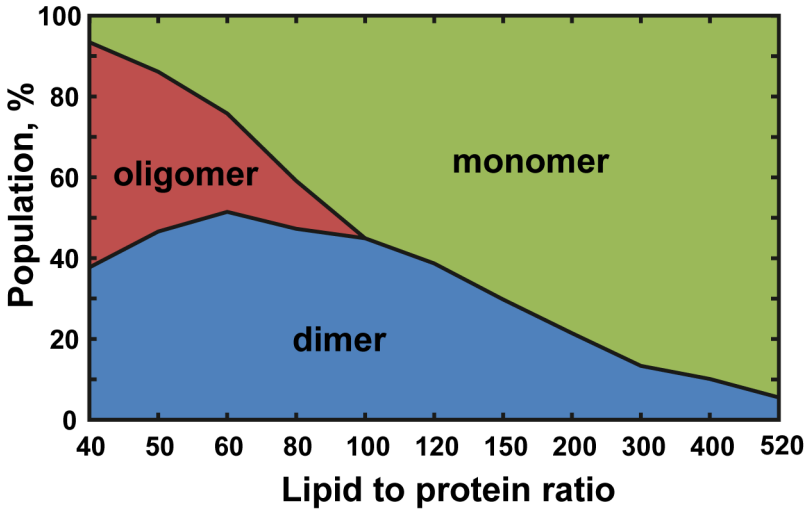
100
80
60
40
20
0
Population, %
oligomer
monomer
dimer
40
50
60
80
100
120
150
200
300
400
520
Lipid to protein ratio

B

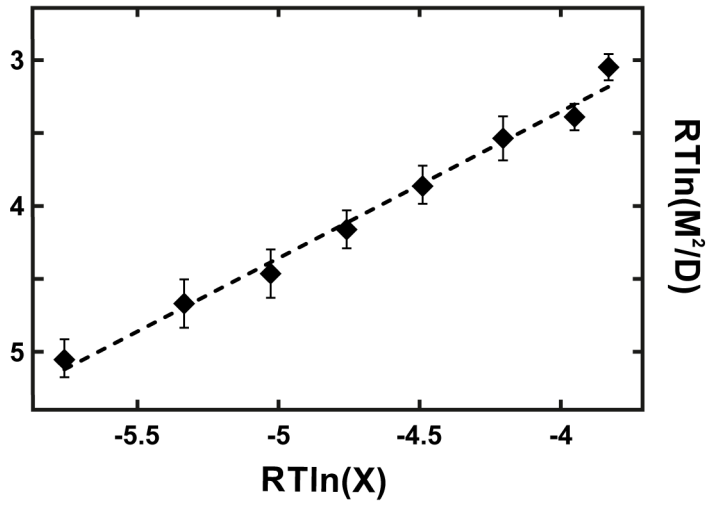
3
4
5
-5.5
-5
-4.5
-4
RTln(X)
RTln(M²/D)

Figure S2

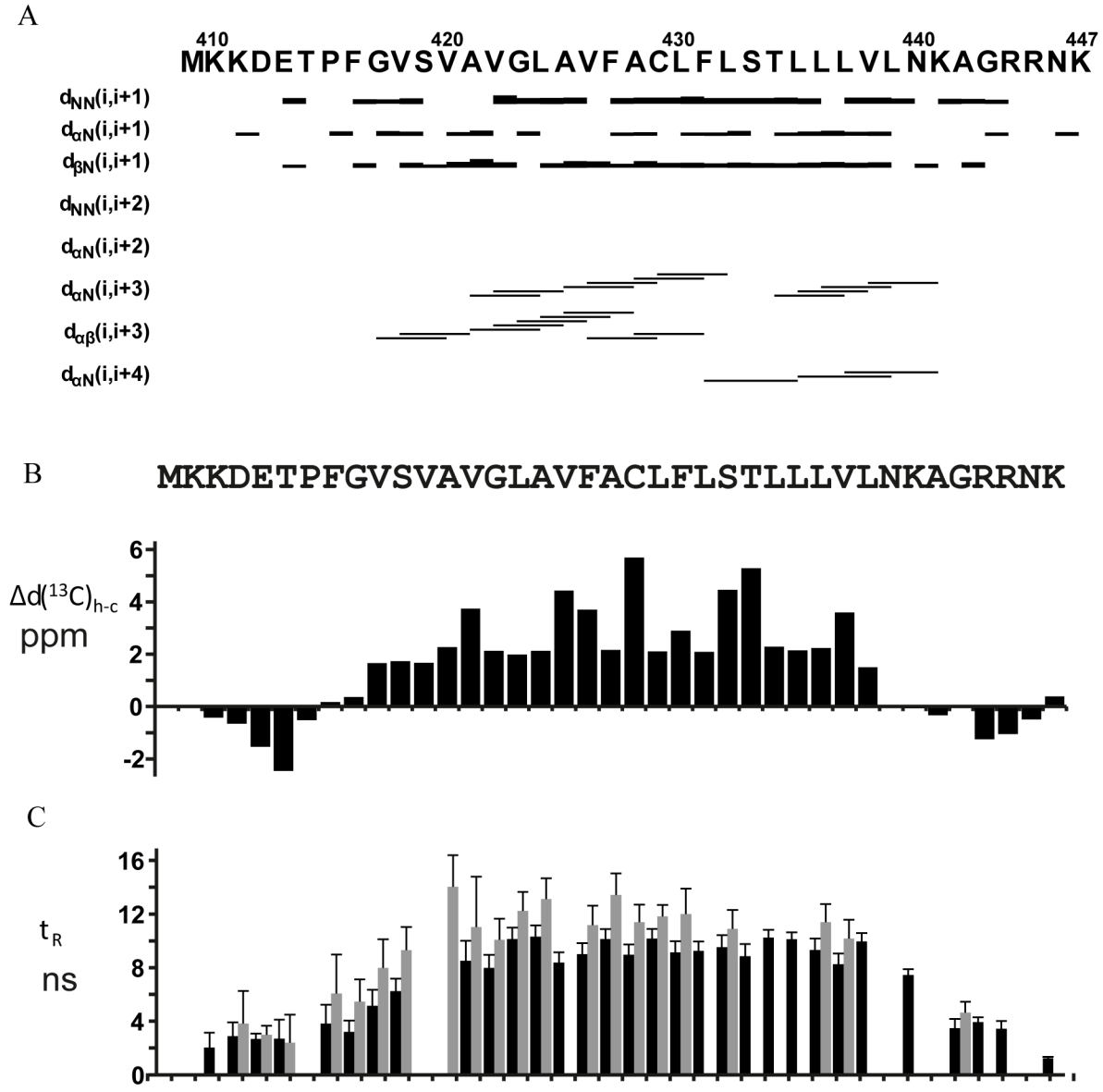
A
410
420
430
440
447
MKKDETPFGVSVAVGLAVFACLFLSTLLLVLNKAGRRNK
$d_{NN}(i,i+1)$
$d_{\alpha N}(i,i+1)$
$d_{\beta N}(i,i+1)$
$d_{NN}(i,i+2)$
$d_{\alpha N}(i,i+2)$
$d_{\alpha N}(i,i+3)$
$d_{\alpha\beta}(i,i+3)$
$d_{\alpha N}(i,i+4)$
B
MKKDETPFGVSVAVGLAVFACLFLSTLLLVLNKAGRRNK
$\Delta d(^{13}C)_{h-c}$ ppm
6
4
2
0
-2
C
t_R ns
16
12
8
4
0

Figure S3

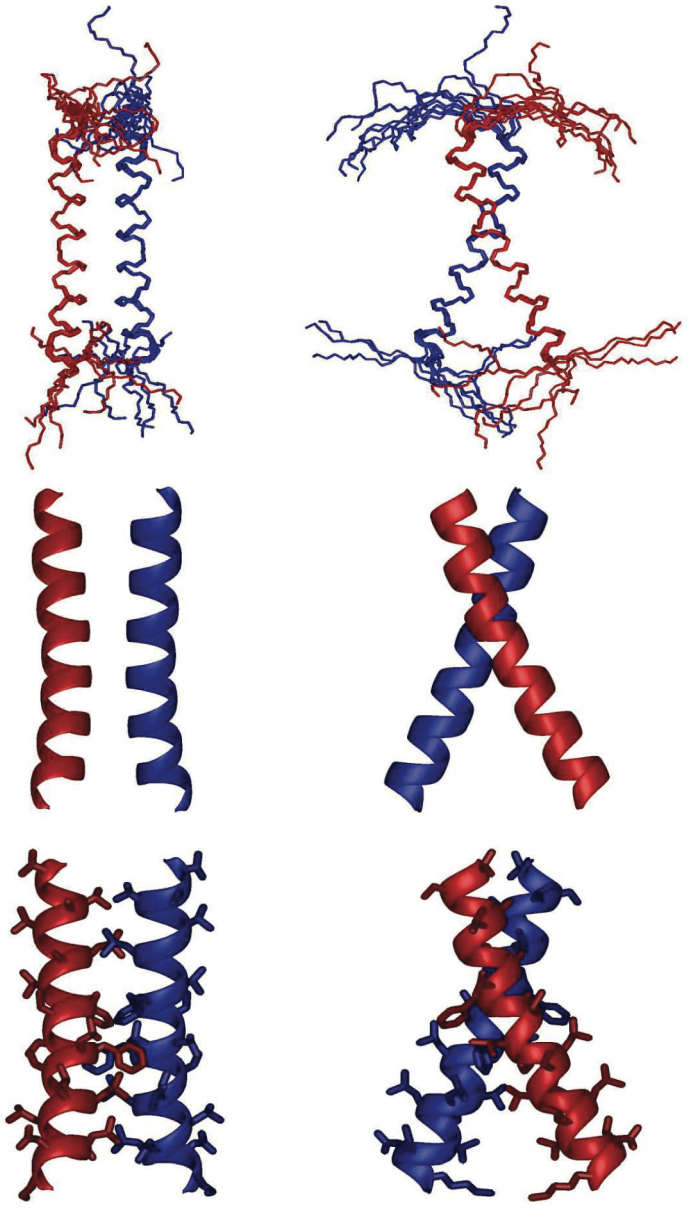

Figure S4

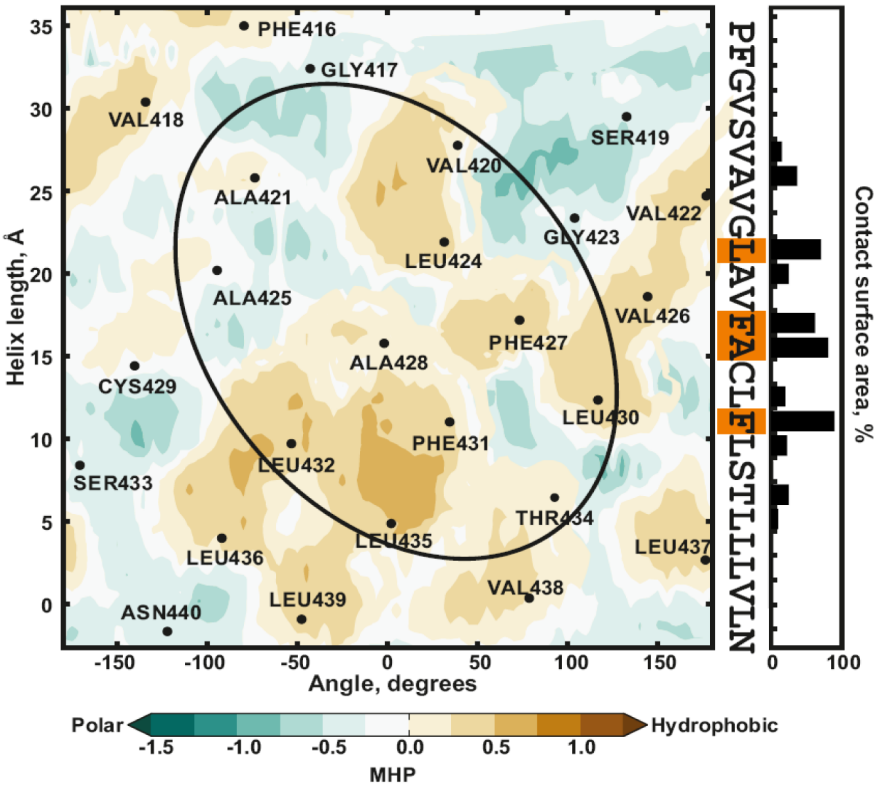
PHE416
GLY417
VAL418
SER419
VAL420
ALA421
VAL422
GLY423
LEU424
ALA425
VAL426
PHE427
ALA428
CYS429
LEU430
PHE431
LEU432
SER433
THR434
LEU435
LEU436
LEU437
VAL438
LEU439
ASN440
Helix length, Å
Angle, degrees
PFGVSVAVGLAVFACLFLSTLILVLN
Contact surface area, %
Polar
Hydrophobic
MHP

Figure S5

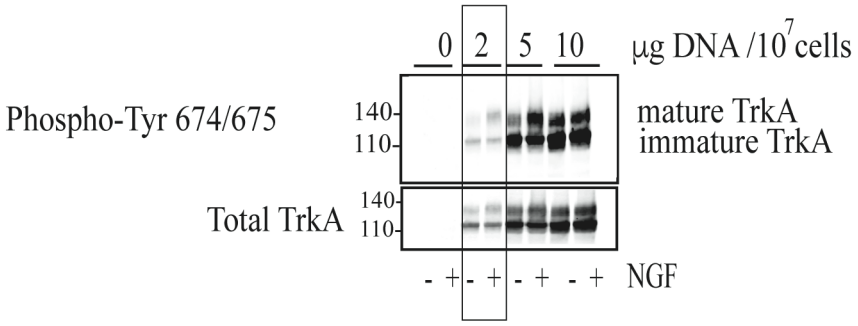
0 2 5 10
μg DNA /10^7 cells
Phospho-Tyr 674/675
140
110
mature TrkA
immature TrkA
Total TrkA
140
110
- + - + - + - + NGF

Figure S6

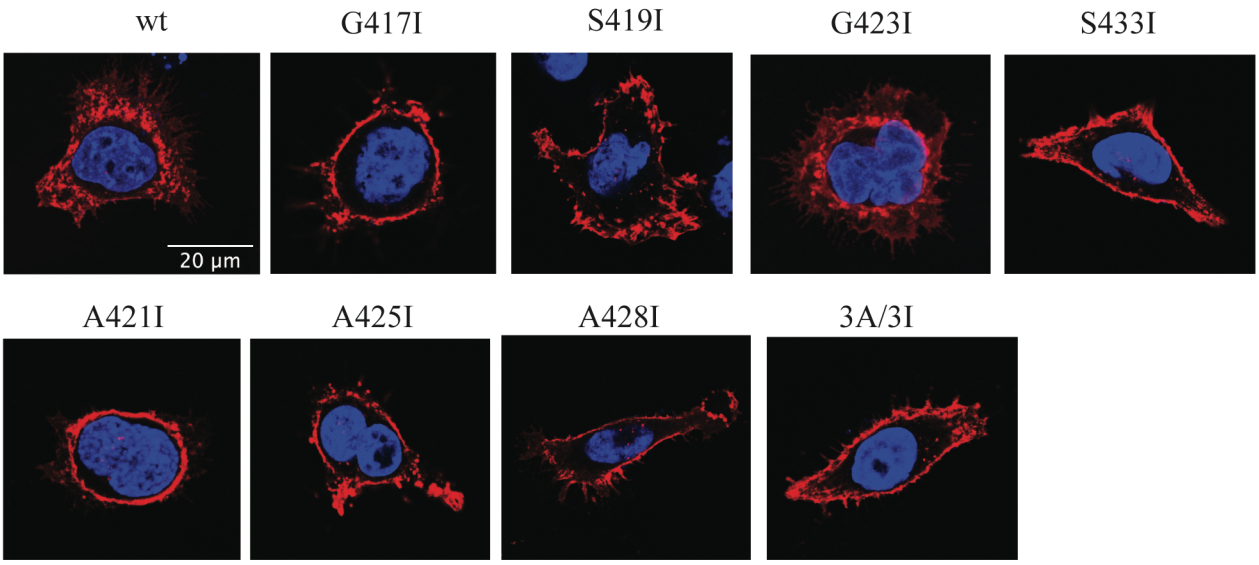

Figure S7

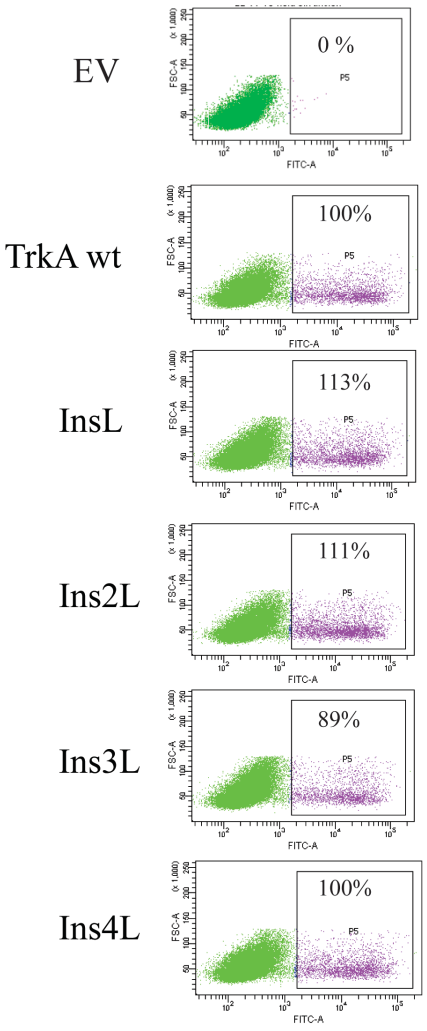
EV
0 %
P5
FSC-A
FITC-A
TrkA wt
100%
P5
InsL
113%
P5
Ins2L
111%
P5
Ins3L
89%
P5
Ins4L
100%
P5